Relaxed energy and structure of edge dislocation in iron*

Zhang Yan(张 研)[a)b)], Xie Li-Juan(解丽娟)[a)], Zhang Jian-Min(张建民)[a)†], and Xu Ke-Wei(徐可为)[c)]

[a)] *College of Physics and Information Technology, Shaanxi Normal University, Xi'an* 710062, *China*

[b)] *Laboratoire SPMS, École Centrale Paris, CNRS-UMR* 8580, 92295 *Châtenay-Malabry Cedex, France*

[c)] *State Key Laboratory for Mechanical Behaviour of Materials, Xi'an Jiaotong University, Xi'an* 710049, *China*

(Received 25 July 2010; revised manuscript received 20 August 2010)

With modified analytical embedded-atom method and molecular dynamics simulation, this paper simulates the strain energy and the equilibrium core structure of $a\langle 100\rangle$ edge dislocation in BCC metal iron on atomistic scale. In addition, the trapping effect of dislocation on vacancy is investigated as well. The results show that the equilibrium dislocation core is quite narrow and has a C_{2v} symmetry structure. Calculated strain energy E_s of the dislocation is a linear function of $\ln(R/2b)$ while $R \geq 5.16$ Å (1 Å = 0.1 nm), in excellent agreement with the elasticity theory prediction. Determined core radius and energy are 5.16 Å and 0.62 eV/Å, respectively. The closer the vacancy to the dislocation line is, the lower the vacancy formation energy is, this fact implies that the dislocation has a trend to trap the vacancy, especially for a separation distance of the vacancy from dislocation line being less than two lattice constants.

Keywords: iron, edge dislocation, vacancy, modified analytical embedded-atom method

PACS: 61.82.Bg, 61.72.Bg, 61.72.Lk, 61.72.Jd **DOI:** 10.1088/1674-1056/20/2/026102

1. Introduction

Iron or steel is one of the important industrial materials. To set up a link between the microstructures and the mechanical properties, it is very important to understand deformation and defect properties of the metals at the atomistic level. For instance, accurate determinations of the structure energy and movement of the dislocations are considered crucial for the understanding of plasticity and crack behaviour of the metals.[1] Although many modern experimental techniques, such as the scanning tunneling microscope (STM), the field ion microscope (FIM), the high-resolution transmission electron microscope (HRTEM), etc., have been used to observe the structures of crystal defects at the atomistic level, many details of these structures remain beyond the scope of these tools.

With the fast development of high-performance computers, atomistic scale simulations based on various physical models[2−6] are becoming a powerful supplement to current experimental methods. Cottrell suggested that $a\langle 100\rangle$ edge dislocation form a microcrack just below its slip plane, and it is therefore likely that this kind of dislocation may play an important role in the process of crack nucleation in BCC materials.[7] The core structure of $a\langle 100\rangle$ dislocation was studied by using the pair-potential theory.[8] In contrast to the pair-potential theory where only the potential energy of a system of particles is considered, one of the many-body models, embedded atom method (EAM) developed by Daw and Baskes,[9,10] presents the energy of an atom in a system as a sum of electrostatic interactions with each of its near neighbours and an energy to embed the atom in the local electron density created by its near neighbours. It is believed that a many-body effect sensitive to the local environment of atoms makes the accurate treatment of defective structures.[11] As an extension to initial EAM and analytical EAM (AEAM) developed by Johnson *et al.*,[12,13] the modified analytical EAM (MAEAM) has been used successfully in calculations for many properties of metals and alloys.[14−17] In our previous papers, the surface energy,[18−20] interface energy[21−24] and grain boundary energy[25−28] have been calculated by MAEAM and many properties related to these face defects have been explained satisfactory.

In this paper, an atomistic investigation of the en-

*Project supported by the State Key Development Program for Basic Research of China (Grant No. 2004CB619302), and the National Natural Science Foundation of China (Grant No. 51071098).

†Corresponding author. E-mail: jianm_zhang@yahoo.com

© 2011 Chinese Physical Society and IOP Publishing Ltd

ergy and structure of $a\langle 100\rangle$ edge dislocation in iron has been made by combining the MAEAM potential with molecular dynamics (MD) method. Further, the trapping effect of dislocation on vacancy was also investigated. The results show that the equilibrium structure of the dislocation core is quite narrow and has C_{2v} symmetry structure. Calculated strain energy of the dislocation is a linear function of $\ln(R/2b)$ while $R \geq 5.16$ Å, this is in excellent agreement with the prediction of elasticity theory. The core radius and energy are determined to be 5.16 Å and 0.62 eV/Å respectively. The formation energy calculations for a vacancy sited in various separation distances from the dislocation line show that the dislocation has a trend to trap the vacancy, especially for the separation distance being less than two lattice constants.

2. The MAEAM

In the MAEAM, the total energy of a system $E_{\rm t}$ is expressed as[17]

$$E_t = \sum_i F(\rho_i) + \frac{1}{2}\sum_i \sum_{j(\neq i)} \varphi(r_{ij}) + \sum_i M(P_i), \tag{1}$$

$$\rho_i = \sum_{j(\neq i)} f(r_{ij}), \tag{2}$$

$$P_i = \sum_{j(\neq i)} f^2(r_{ij}), \tag{3}$$

where $F(\rho_i)$ is the energy to embed atom i in its site with electron density ρ_i given by a linear superposition of spherical averaged atomic electron density of the other atoms $f(r_{ij})$, r_{ij} is the separation distance of atom j from atom i, $\varphi(r_{ij})$ is the interaction potential between atoms i and j, and $M(P_i)$ is the modified term, which describes the energy change due to non-spherical distribution of electrons (P_i) and deviation from the linear superposition of atomic electronic density. Embedding function $F(\rho_i)$, pair potential $\varphi(r_{ij})$, modified term $M(P_i)$, and atomic electron density $f(r_{ij})$ take the following forms:[17]

$$F(\rho_i) = -F_0\left[1 - n\ln(\rho_i/\rho_{\rm e})\right](\rho_i/\rho_{\rm e})^n, \tag{4}$$

$$\varphi(r_{ij}) = k_0 + k_1\left(r_{ij}/r_{1{\rm e}}\right)^2 + k_2\left(r_{ij}/r_{1e}\right)^4 + k_3\left(r_{1{\rm e}}/r_{ij}\right)^{12}, \tag{5}$$

$$M(P_i) = \alpha\left(P_i/P_{\rm e} - 1\right)^2 \exp\left[-\left(P_i/P_{\rm e} - 1\right)^2\right], \tag{6}$$

$$f(r_{ij}) = f_{\rm e}(r_{1{\rm e}}/r_{ij})^6, \tag{7}$$

where subscript e indicates equilibrium and $r_{1{\rm e}}$ is the first nearest neighbouring distance at equilibrium. In this paper, the electron density at equilibrium $f_{\rm e}$ is chosen as

$$f_{\rm e} = \left[(E_{\rm c} - E_{1{\rm f}})/\Omega\right]^{3/5}, \tag{8}$$

where $\Omega = a^3/2$ is the atomic volume in BCC metals, a is the lattice constant.

Seven parameters F_0, n, k_0, k_1, k_2, k_3 and α in Eqs. (4)–(6) can be determined by fitting lattice constant a, cohesion energy $E_{\rm c}$, monovacancy formation energy $E_{1{\rm f}}$, and elastic constants C_{11}, C_{12} and C_{44} of specific metals. According to the principle that the energy vs. separation distance curve fits the Rose equation,[29] we have

$$F_0 = E_{\rm c} - E_{1{\rm f}}, \tag{9}$$

$$n = \sqrt{\Omega(C_{11} + 2C_{12})(C_{11} - C_{12})/(216E_{1{\rm f}}C_{44})}, \tag{10}$$

$$\alpha = \Omega\left(C_{12} - C_{44}\right)/32 - n^2F_0/8. \tag{11}$$

The potential parameters can be calculated with the following formulae[17]

$$k_0 = -\frac{E_{1{\rm f}}}{7} - \frac{\Omega(51519C_{44} + 57111C_{12} - 57111C_{11})}{471800}, \tag{12}$$

$$k_1 = \frac{\Omega(33327C_{44} + 52563C_{12} - 52563C_{11})}{269600}, \tag{13}$$

$$k_2 = \frac{\Omega(147456C_{11} - 147456C_{12} - 59049C_{44})}{1887200}, \tag{14}$$

$$k_3 = \frac{1536\Omega(4C_{44} - C_{11} + C_{12})}{412825}. \tag{15}$$

Substituting lattice constant a, cohesion energy $E_{\rm c}$, monovacancy formation energy $E_{1{\rm f}}$, and elastic constants C_{11}, C_{12} and C_{44} of iron[17] listed in Table 1 into Eqs. (9)–(15), we obtain seven parameters needed for energy calculation listed in Table 2. Substituting the values of k_i (i = 0–3) into Eq. (5), we plot the interatomic potential for iron in Fig. 1. To test the model, the formation energy of an octahedron interstitial atom is calculated to be 4.79 eV which nearly equals the value of 4.77 eV calculated by Harder and Bacon.[30]

Table 1. Physical parameters of iron.[17]

a/Å	$E_{\rm c}$/eV	$E_{1{\rm f}}$/eV	C_{11}/GPa	C_{12}/GPa	C_{44}/GPa
2.8665	4.29	1.79	230	135	117

Table 2. Calculated parameters of iron for MAEAM.

F_0/eV	n	α	k_0/eV	k_1/eV	k_2/eV	k_3/eV
2.50000	0.27801	0.01725	−0.34966	−0.29874	0.27690	0.10215

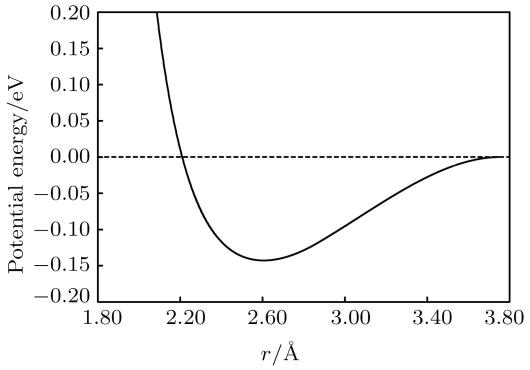


Fig. 1. The curve of interatomic potential of iron.

3. Computational procedures

A BCC super-cell is used in computation of the long-range strain field induced by a dislocation. The size of the model crystal is a $66a \times 30a \times 7.5a$ lattice block with 29700 atoms, where a is the lattice constant. The number of atomic planes in the $\langle 100\rangle$, $\langle 010\rangle$ and $\langle 001\rangle$ directions are 133, 61 and 16, respectively. An $a\langle 100\rangle$ edge dislocation is initialized by displacing the atoms according to the elasticity theory. The model crystal is divided into two regions: an inner region and an outer region. The dislocation core is contained in the inner region, where atomic positions are fully relaxed according to atomic stress. The outer region surrounds the inner region where atomic positions are fixed according to the initial displacements. The mantle ensures that each atom in the inner computational region has a complete set of neighbours within the range of the used interatomic potential. The lattice relaxations resulted from the existences of the dislocation and vacancy are simulated with the MD method[31] at constant-temperature of 0 K. In which the coordinate of the i-th atom $\boldsymbol{r}_i$ is assumed as a function of time. While the increment of time Δt is infinitesimal, the $\boldsymbol{r}_i$ can be expanded by a Taylor series. The coordinate $\boldsymbol{r}_i(t+\Delta t)$ of atom i at time $t+\Delta t$ can be obtained from the coordinate $\boldsymbol{r}_i(t)$ of the atom at time t by a predictor–corrector method,[32]

$$\boldsymbol{r}_i^{\in}(t+\Delta t) = \boldsymbol{r}_i(t) + \dot{\boldsymbol{r}}_i(t)\Delta t + \frac{1}{2}\frac{\boldsymbol{f}_i(\boldsymbol{r}_i)}{m}\Delta t^2, \quad (16)$$

repeating l times

$$\begin{cases} \boldsymbol{r}_i(t+\Delta t) = \boldsymbol{r}_i(t) + \dot{\boldsymbol{r}}_i(t+\Delta t)\Delta t + \dfrac{1}{2}\dfrac{\boldsymbol{f}_i(\boldsymbol{r}_i^{\in})}{m}\Delta t^2, \\ \boldsymbol{r}_i^{\in}(t+\Delta t) = \boldsymbol{r}_i(t+\Delta t), \end{cases} \quad (17)$$

where $\boldsymbol{r}_i^{\in}(t+\Delta t)$ is the coordinate predicted at time $t+\Delta t$, $\dot{\boldsymbol{r}}_i(t) = \mathrm{d}\boldsymbol{r}_i(t)/\mathrm{d}t$ is the velocity of atom i at time t, $\boldsymbol{f}_i(\boldsymbol{r}_i) = \mathrm{d}E_i/\mathrm{d}\boldsymbol{r}_i$ is the resultant force applied to atom i from the other atoms at time t, and m is the mass of the atom. E_i is the energy of atom i. In this paper, we take $l = 3$ and $\Delta t = 1$ fs.

The strain energy of an edge dislocation is the superabundance relative to bulk material due to the existence of the dislocation. Thus a contribution to the strain energy of the dislocation by atom i can be shown as $E_i - E_\mathrm{b}$, here

$$E_i = F(\rho_i) + \frac{1}{2}\sum_{j(\neq i)}\varphi(r_{ij}) + M(P_i)$$

is the energy of the atom i after relaxation, E_b is the energy of an atom in perfect bulk crystal and equals the negative value of cohesive energy. Summing all contributions of atoms within inner computational region and then dividing it by the length L of dislocation line, we can obtain the strain energy of the dislocation per unit length E_s

$$E_s = \frac{1}{L}\sum_{i=1}^{n}(E_i - E_\mathrm{b}), \quad (18)$$

where n is the number of atoms inside the inner computational region.

The formation energy of a vacancy near the dislocation core E_v^f can be calculated by

$$E_\mathrm{v}^\mathrm{f} = E_\mathrm{d+v}^\mathrm{tot} - E_\mathrm{d}^\mathrm{tot} - E_\mathrm{c}, \quad (19)$$

where $E_\mathrm{d+v}^\mathrm{tot}$ and $E_\mathrm{d}^\mathrm{tot}$ are the total energies of the relaxed edge dislocation with and without the vacancy, respectively, E_c is cohesion energy.

4. Results and discussion

4.1. Structure of $a\langle 100\rangle$ edge dislocation

For $a\langle 100\rangle$ edge dislocation in BCC metals, where a is the lattice constant and also the magnitude of the Burgers vector, the repeated distance along the dislocation line is two crystal planes thus a periodic boundary condition can be used to simulate the simultaneous relaxation of the equivalent atoms along infinite long dislocation line. In order to calculate the structure and energy of the dislocation, we construct a cylinder with the edge dislocation line as its axis, which is along $\langle 001\rangle$ direction and is taken here as the z axis. The x and y directions are chosen along $\langle 100\rangle$ and $\langle 010\rangle$ directions respectively (see Fig. 2). In the z direction, a periodic boundary condition is applied as mentioned above. While in the x and y directions, we

use fixed boundary conditions. The stable configuration, as shown in Fig. 2 (a), is obtained after 1×10^5 time steps of runs. The dislocation line is normal to the plane of the figure. Its periodic structure unit along the dislocation line is plotted in Fig. 2 (b).

In Fig. 2, the A plane, on which the atoms are shown with open circles, is created by simultaneous dissociation of one (100) plane into two half-planes above slip plane, while the B plane, on which the atoms are shown with solid rhombus, is then created by introducing an extra (100) half-plane between dissociated two half-planes. Although the A and B planes have different atom arrangements, either of them can be recognized as being composed of corner or body-centre atoms in the BCC lattice, hence they are equal in status. The atoms in core structure unit along the dislocation line are labeled as well. It can be seen that the completely relaxed $a\langle 100\rangle$ dislocation structure has the following three principal characteristics: the first one is the dislocation having a very narrow core region which is consistent with the general character of the BCC metals, the second is the relatively large displacements occurring on the two sides below the slip plane, and the third is the dislocation structure having a C_{2v} symmetry structure.

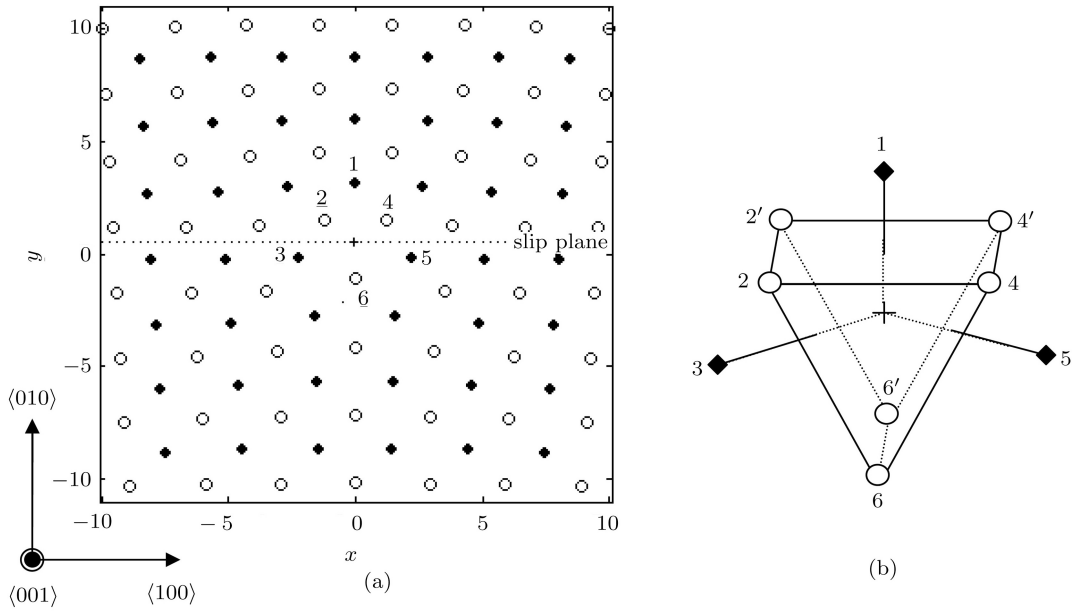


Fig. 2. (a) Completely relaxed configuration of $a\langle 100\rangle$ edge dislocation core in iron; (b) the periodic structure unit along the dislocation line. The open circles and solid rhombus represent the atoms on two adjacent A and B planes perpendicular to $\langle 001\rangle$ direction. The cross symbol represents the vacancies in the centre of dislocation. Atoms around the dislocation line are numbered.

4.2. Energy of $\langle 100\rangle$ edge dislocation

In order to investigate the effect region of the $a\langle 100\rangle$ edge dislocation from the viewpoint of energy, the energy per atom has been calculated firstly by using the MAEAM potential and MD simulation. The partial results are shown in Figs. 3(a) and 3(b) respectively for the first four rows of the atoms above and below slip plane. The numbers in the two figures correspond to the atoms labeled in Fig. 2. We can see that the distribution of energy has very good symmetry in the $\langle 100\rangle$ direction, which is consistent with C_{2v} symmetry of the above structure. It is noted that from Fig. 3(a), above slip plane the energy of the second and fourth atoms on the first row are -4.0104 eV, which is 0.28 eV higher than the energy of an atom in perfect bulk crystal $E_{\rm b}$ (-4.29 eV). The energy of the first atom on the second row decreases to -4.1796 eV, which is only 0.11 eV higher than $E_{\rm b}$. Moreover, the difference between the energy of the fourth row atoms and $E_{\rm b}$ is less than 0.02 eV, although there exists an energy fluctuation among the atoms within two lattice constants away from the extra half atom plane in the $\langle 100\rangle$ direction. The similar conclusions can also be obtained for the region below the slip plane in Figs. 3(b) excepting that the effect region is one lat-

tice constant broader than that above the slip plane, although the energy of the third and fifth atoms on the first row below the slip plane is lower than that of the second and fourth atoms on the first row above the slip plane. Therefore figure 3 gives a vivid picture of the effect region of the $a\langle 100\rangle$ edge dislocation from the viewpoint of energy. If the energy of an atom is within 0.02 eV (0.5%) tolerance of the energy of an atom in perfect bulk crystal $E_{\rm b}$, it may be regarded as an atom situated in perfect crystal, so the determined effect region is about two to three lattice constants around dislocation line. In fact, the energy of all atoms in a relatively large region is higher than the energy of an atom in perfect bulk crystal $E_{\rm b}$, and the farther the atom from the dislocation line is, the lower the atom energy is.

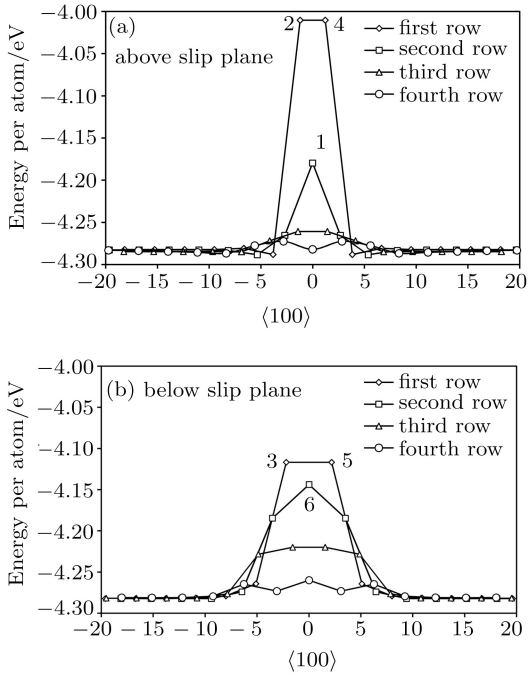


Fig. 3. The energy per atom calculated by MAEAM potential for edge dislocation.

In the general elasticity theory, the total strain energy $E_{\rm s}$ of a dislocation includes two parts: elastic energy ($E_{\rm e}$) and core energy ($E_{\rm core}$). The former can be calculated by using linear elasticity theory. The core energy is the energy contained close to the dislocation line, where due to the large strain, the linear elasticity theory is not valid and the details of the interatomic interactions are important.[33] For an edge dislocation, the total strain energy per repeated distance can be expressed as

$$E_{\rm s} = E_{\rm e} + E_{\rm core} = K\ln(R/r_{\rm c}) + E_{\rm core}, \qquad (20)$$

where R is the outer cutoff radius of a cylinder which contains the dislocation core at its centre, the inner cutoff radius $r_{\rm c}$ is defined as the core radius, K depends on the elastic constants,[34]

$$K = (b^3/4\pi)(C_{11}+C_{12}) \times [C_{44}(C_{11}-C_{12})/C_{11}(C_{11}+C_{12}+2C_{44})]^{1/2}, \qquad (21)$$

where b is Burgers vector. Inserting the values of three elastic constants listed in Table 1, we can obtain K=1.2187 eV. To make a quantitative correspondence between Eq. (20) and our calculated results, we have first tentatively set $r_{\rm c} = 2b$, with $b = a = 2.8665$ Å, the approximate expected value of the core radius. The strain energies $E_{\rm s}$ of the $a\langle 100\rangle$ edge dislocation then have been calculated by using Eq. (18) as a function of the radius R of a cylinder which contains the dislocation core. We define this cylinder to coincide with the inner region of our simulation cell, so that the axis of the cylinder passes through the dislocation core centre. By increasing the radius R, we have thereby generated a plot of linear density of the dislocation strain energy $E_{\rm s}$ versus $\ln(R/2b)$, as displayed in Fig. 4. In

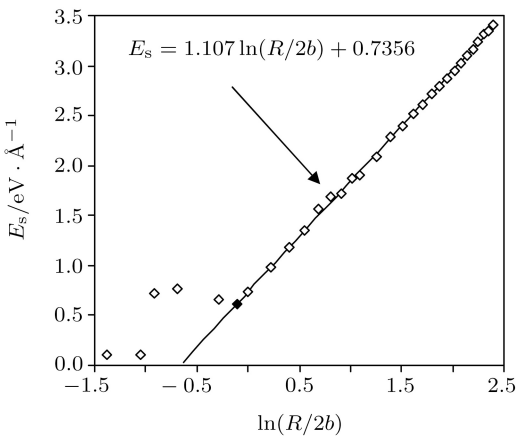


Fig. 4. Plot of $E_{\rm s}$ vs. $\ln(R/2b)$. The fitted points above $\ln(R/2b) = -0.1054$ are shown as a solid straight line.

this plot it is clear that there is a large amount of scatters for small values of R. When $\ln(R/2b) \geq -0.1054$, however, the strain energies follow a straight line as predicted by elasticity theory (Eq. (19)). At that initial point, $R = 1.8b$, which is smaller than the assumed value of $2b$ for the core radius, showing that the value chosen for the core radius $r_{\rm c} = 2b$ is large enough to take account for the non-elastic region near the dislocation line. From a linear fit to our data we

determine the core radius $r_c = 1.8b = 5.16$ Å, the corresponding linear density of the core energy E_{core} is about 0.62 eV/Å. The slope of fitted straight line is 1.107 eV, which is in good agreement with the calculated value of 1.2187 eV.

4.3. Trapping effect of edge dislocation on vacancy

Based on the initial model crystal with an associated vacancy on the dislocation line as described in subsection 4.1, an atom is removed then leaves a vacancy in periodic structure unit. The vacancy is located immediately above the slip plane (on the compression side), and the separation between the vacancy and the dislocation line is varied for the purpose of studying the trapping effect of the edge dislocation on the vacancy. In fact, the periodic boundary condition along the dislocation line requires that a line of the vacancies is actually being simulated. The size of the relaxed region is $60a$ in $\langle 100 \rangle$ direction, $14a$ in the $\langle 010 \rangle$ direction, and $3.5a$ in the $\langle 001 \rangle$ direction, this fact corresponds to 6720 atoms. The dislocation line penetrates the centre of this region. The simulations are performed with MD method. The formation energies of a vacancy near dislocation core

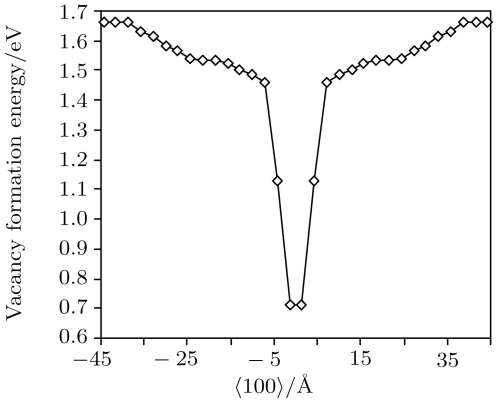


Fig. 5. The vacancy formation energy E_v^f near the edge dislocation line in iron.

E_v^f are calculated by Eq. (19). Figure 5 shows the relation of E_v^f and the x-coordinates of the vacancy. The fact, that the closer the vacancy to the dislocation line is, the lower the formation energy is, implies the dislocation has a trend to trap the vacancy, especially for the separation distance of the vacancy from dislocation line is less than two lattice constants. From the formation energies of a vacancy sited far away from the dislocation line 1.66 eV and immediately near the dislocation line (position 2 or 4 in Fig. 2(a)) 0.71 eV, respectively, we know $a\langle 100 \rangle$ edge dislocation has a relatively strong ability to trap a vacancy.

5. Conclusions

Using combined MAEAM potential with MD method, we have calculated systematically the relaxed strain energy and the structure of $a\langle 100 \rangle$ edge dislocation in BCC metal iron. In addition, the trapping effect of dislocation on vacancy was investigated as well. The completely relaxed $a\langle 100 \rangle$ dislocation has the following three structural characteristics. First, the dislocation has a very narrow core region, which is consistent with the general character of the BCC metals. Secondly, the relatively large displacements occur for the atoms near dislocation line especially for the atoms on the two sides below the slip plane. Thirdly, the dislocation structure has a C_{2v} symmetry. These structural characteristics are also reflected in energy. A linear fitting of the calculated strain energy E_s with $\ln(R/2b)$ gives the dislocation core radius $r_c = 5.16$ Å and the core energy E_{core}=0.62 eV/Å. The formation energy calculations for a vacancy sited in various separation distances from the dislocation line show that the dislocation has a trend to trap the vacancy, especially for the separation distance of the vacancy from dislocation line is less than two lattice constants.

References

[1] Xu W and Moriarty J A 1996 *Phys. Rev.* B **54** 6941
[2] Voskoboinikov R E, Osetsky Y N and Bacon D J 2005 *Mater. Sci. Eng.* A **400** 45
[3] Bodur C T, Chang J and Argon A S 2005 *J. Euro. Ceram. Soc.* **25** 1431
[4] Dang H L and Wang C Y 2007 *Comput. Mater. Sci.* **39** 557
[5] Clouet E 2006 *Acta Mater.* **54** 3543
[6] Heinisch H L, Gao F, Kurtz R J and Le E A 2006 *J. Nucl. Mater.* **351** 141
[7] Cottrell A H 1958 *Trans. Met. Soc. AIME* **212** 192
[8] Ohr S M and Beshers D N 1963 *Philos. Mag.* **8** 1343
[9] Dow M S and Baskes M I 1983 *Phys. Rev. Lett.* **50** 1258
[10] Dow M S and Baskes M I 1984 *Phys. Rev.* B **29** 6443
[11] Seki A, Hellman O and Tanaka S I 1996 *Script. Metal.* **34** 1867
[12] Johnson R A 1988 *Phys. Rev.* B **37** 3924
[13] Johnson R A and Oh D J 1989 *J. Mater. Res.* **4** 1195

[14] Zhang B W and Ouyang Y F 1993 *Phys. Rev.* B **48** 3022
[15] Zhang B W, Ouyang Y F, Liao S Z and Jin Z P 1999 *Physica* B **262** 218
[16] Hu W Y, Zhang B W, Huang B Y, Gao F and Bacon D J 2001 *J. Phys.: Condens. Matter* **13** 1193
[17] Hu W Y, Zhang B W, Shu X L and Huang B Y 1999 *J. Alloys Compd.* **287** 159
[18] Zhang J M, Ma F and Xu K W 2004 *Appl. Surf. Sci.* **229** 34
[19] Zhang J M, Ma F and Xu K W 2003 *Surf. Interf. Anal.* **35** 662
[20] Zhang J M, Ma F, Xu K W and Xin X T 2003 *Surf. Interf. Anal.* **35** 805
[21] Ma F, Zhang J M and Xu K W 2004 *Surf. Interf. Anal.* **36** 355
[22] Xin H, Zhang J M, Wei X M and Xu K W 2005 *Surf. Interf. Anal.* **37** 608
[23] Zhang J M, Xin H and Wei X M 2005 *Appl. Surf . Sci.* **246** 14
[24] Zhang J M, Xin H and Wei X M 2005 *Acta Phys. Sin.* **54** 237 (in Chinese)
[25] Zhang J M, Wei X M, Xin H and Xu K W 2005 *Chin. Phys.* **14** 1015
[26] Zhang J M, Wei X M and Xin H 2004 *Surf. Interf. Anal.* **36** 1500
[27] Zhang J M, Wei X M and Xin H 2005 *Appl. Surf. Sci.* **243** 1
[28] Zhang J M, Huang Y H, Xu K W and Ji V 2007 *Chin. Phys.* **16** 210
[29] Rose J H, Smith J R, Guinea F and Ferante J 1984 *Phys. Rev.* B **29** 2963
[30] Harder J M and Bacon D J 1988 *Philos. Mag.* A **58** 165
[31] Smith R W and Srolovitz D J 1996 *J. Appl. Phys.* **79** 1448
[32] Beeler Jr J R 1983 *Radiation Effects Computer Experiments* (Amsterdam: North-Holland) p. 128
[33] Gilman J J 2005 *Mater. Sci. Eng.* A **409** 7
[34] Gehlen P C, Rosenfield A R and Hahn G T 1968 *J. Appl. Phys.* **39** 5246